Verification of the vibrational exciton approach for CO[sub 2] and N[sub 2]O nanoparticles

Originally published in:
The Journal of Chemical Physics 118(6), https://doi.org/10.1063/1.1531622

Verification of the vibrational exciton approach for CO_2 and N_2O nanoparticles

Cite as: J. Chem. Phys. **118**, 2707 (2003); https://doi.org/10.1063/1.1531622
Submitted: 17 September 2002 . Accepted: 30 October 2002 . Published Online: 23 January 2003

Ruth Signorell

Verification of the vibrational exciton approach for CO_2 and N_2O nanoparticles

Ruth Signorell[a)]
Institut für Physikalische Chemie, Universität Göttingen, Tammannstr. 6, D-37077 Göttingen, Germany

(Received 17 September 2002; accepted 30 October 2002)

It is investigated how far the vibrational exciton approximation is suitable to describe the characteristic band shapes in the infrared spectra of CO_2 and N_2O nanoparticles. The particles typically contain between 50 and 10^4 molecules and have spatial dimensions between 1 and 10 nm. The accuracy of the exciton approach is estimated by comparison with experimental data and quantum chemical calculations for small clusters. The spectral changes due to different particle shapes and particle sizes are investigated with respect to the estimated accuracy. This includes the determination of a typical effective range for the dipole–dipole coupling. © *2003 American Institute of Physics.* [DOI: 10.1063/1.1531622]

I. INTRODUCTION

Aggregates of CO_2 and N_2O belong to the best studied van der Waals-bonded systems. These are among the few particulate systems where experimental studies really cover the whole size range from small clusters[1–17] to nanoparticles[6,12,13,18–25] and beyond.[24,26–30] In a recent experimental infrared study, we have been able to bridge the gap between molecular clusters and large particles.[24,31] This covers the particularly interesting range between 1 and 10 nm, where surface effects are expected to play a major role.

The analysis of the infrared spectra of these nanoparticles requires a suitable model. Quantum chemical methods used so far[25] reach their limit already for the smallest particles with sizes around 1 nm. For the larger particles, the approach has to be simplified by reducing it to the dominant contributions, which determine the vibrational spectra. For the crystalline bulk state of CO_2 and N_2O, it was earlier assumed that the dominant contribution to the infrared spectra comes from the resonant coupling of the oscillating dipoles of the individual molecules.[32–38] This so-called exciton approach indeed produced reasonable agreement with the experimental infrared spectra of the bulk. The exciton model was also used to describe the infrared spectra of clusters containing up to several hundred molecules.[39–41] Due to the finite size, the spectra of the particulate systems show noticeably more structured band shapes than the spectra of the corresponding bulk. This makes it a much more demanding task to simulate these spectra in detail so that it is not obvious that approaches used for bulk spectra can be transferred to particulate matter. Therefore, it is most important to clarify the suitability of the exciton approach for infrared spectra of particulate CO_2 and N_2O. Such a systematic investigation, however, has so far been missing.

The aim of the present study is to fill this gap and to put the exciton model on a sound and quantitative footing. This also includes the extension of this approach to the nanometer size range up to diameters of about 10 nm. In Sec. III, the accuracy of the exciton approach is estimated by comparison with experimental data and quantum chemical calculations for small clusters. The effects of different particle shapes and particle sizes on the infrared spectra of CO_2 and N_2O nanoparticles are discussed in Sec. IV. For nanoparticles, these effects are closely related to the typical effective range of the dipole–dipole coupling. The present study focuses on the antisymmetric-stretching vibration (ν_3) of CO_2, the N–N-stretching vibration (ν_3) of N_2O, and N–O-stretching vibration (ν_1) of N_2O.

II. CALCULATIONS

A. Vibrational exciton calculations

The infrared active stretching fundamentals of CO_2 and N_2O become broad structured band systems upon the aggregation of the molecules. The explanation of this effect in terms of resonant dipole–dipole coupling between the individual aggregated molecules goes back to a study of Hexter in 1960.[38] The dipole–dipole coupling leads to splittings of the degenerate energy levels of the individual molecules and accordingly to a mixing of their local wave functions. The following derivation is analogous to that given by Hexter for crystalline bulk states. The difference is that for nanoparticles all pairwise dipole–dipole interactions have to be considered explicitly. In this case, the vibrational Hamiltonian has the following form:

$$\hat{H} = \hat{H}_0 + \hat{H}_D \tag{1}$$

with

$$\hat{H}_0 = \sum_{i=1}^{N} \hat{H}_{0i} \tag{2}$$

and

$$\hat{H}_D = \sum_{i<j} -\frac{1}{4\pi\epsilon_0} \boldsymbol{\mu}_i \cdot \frac{3(\boldsymbol{\mu}_j \cdot \mathbf{r}_{ij}) \cdot \mathbf{r}_{ij} - (\mathbf{r}_{ij} \cdot \mathbf{r}_{ij}) \cdot \boldsymbol{\mu}_j}{r_{ij}^5}. \tag{3}$$

a)Fax: +49 551-393117; Electronic mail: rsignor@gwdg.de

N is the number of molecules and $\hat{H}_0$ is the sum over the vibrational Hamiltonians $\hat{H}_{0i}$ of the uncoupled molecules. $\hat{H}_D$ includes all pairwise dipole–dipole interactions between the molecules in the aggregate. $\mathbf{r}_{ij}$ is the vector connecting the centers-of-mass of the two molecules labeled i and j. r_{ij} is the corresponding distance. For the dipole moment operators $\boldsymbol{\mu}_i$, only the first derivatives with respect to the normal coordinate Q_i are considered,

$$\boldsymbol{\mu}_i = \boldsymbol{\mu}_{0i} + \left(\frac{\partial \boldsymbol{\mu}_i}{\partial Q_i} \right)_{Q_i=0} \cdot Q_i . \tag{4}$$

The Hamilton matrix is calculated in the product basis,

$$|0\rangle = \prod_i |\varphi_{0i}\rangle \tag{5}$$

and

$$|1_i\rangle = |\varphi_{01}\rangle \cdots |\varphi_{1i}\rangle \cdots |\varphi_{0N}\rangle . \tag{6}$$

φ_{0i} is the ground state of the uncoupled molecule labeled i and φ_{1i} is its first excited state. The Hamilton matrix includes only resonant interactions between states with one quantum of excitation [Eq. (6)]. The eigenvalues $\tilde{\nu}_n$ and the eigenfunctions (or exciton wave functions) ψ_n are obtained by diagonalization. The intensity (integrated line strength) S_n of each vibrational transition is calculated to be

$$S_n \propto \langle 0 | \sum_i \boldsymbol{\mu}_i | \psi_n \rangle^2 \cdot \tilde{\nu}_n . \tag{7}$$

If all uncoupled molecules are equivalent, the model contains two parameters: the transition wave number of the uncoupled molecules

$$\tilde{\nu}_M = \tilde{\nu}_{Mi} \tag{8}$$

and the transition dipole moment of the uncoupled molecules

$$d_M = \langle \varphi_{0i} | \boldsymbol{\mu}_i | \varphi_{1i} \rangle . \tag{9}$$

For the comparison with experimental data in Secs. III and IV, the experimental values of gas phase CO_2 and N_2O are used for $\tilde{\nu}_M$ and d_M. For the comparison with quantum chemical calculations in Sec. III, both parameters are taken from a corresponding quantum chemical calculation for the isolated molecule.

B. Quantum chemical calculations

In Sec. III, the exciton calculations for small aggregates of CO_2 and N_2O are compared with various quantum chemical calculations. This includes semiempirical calculations using the Austin-Model 1 (AM1), density functional theory (B3LYP: Becke three parameter Lee–Yang–Parr), and second order Møller–Plesset (MP2) perturbation theory. For the B3LYP and MP2 calculations, different basis sets ranging from 6–31+G* quality to basis sets with triple-ζ quality including polarization functions have been used. All quantum chemical calculations were performed with the GAUSSIAN program package.[42] The DFT calculations employed integration grids of 75 radial shells with 302 angular points each, pruned to about 7000 grid points per atom. The MP2 calculations included only valence orbitals (frozen core approximation). For the SCF-calculations and the optimizations the tight convergence option were used.

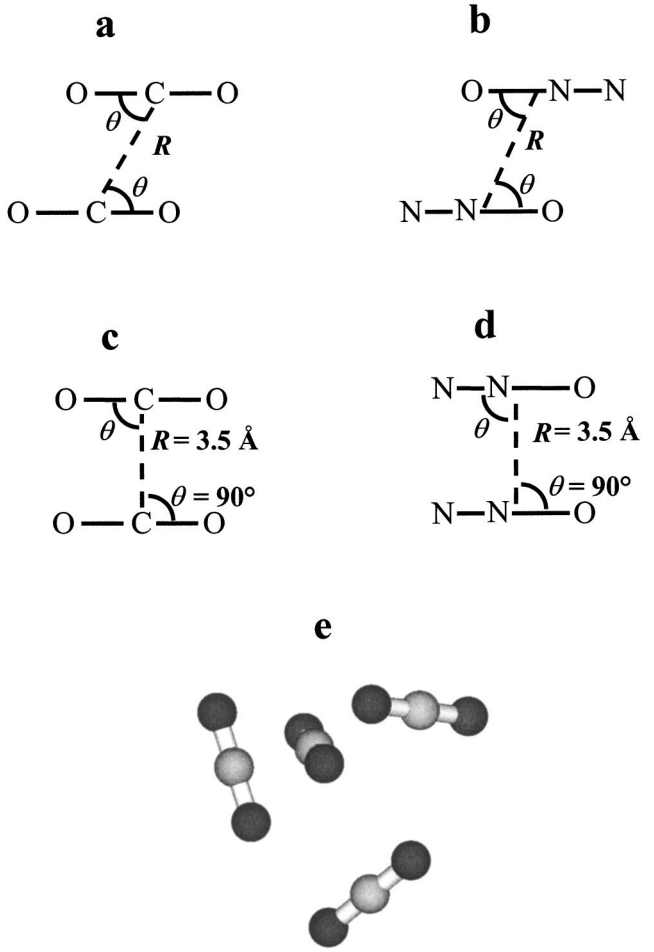

FIG. 1. Geometries of small CO_2 and N_2O clusters. (a) Slipped-parallel CO_2 dimer of C_{2h} symmetry. (b) Slipped-antiparallel N_2O dimer of C_{2h} symmetry. (c) Parallel CO_2 dimer of D_{2h} symmetry. (d) Parallel N_2O dimer of C_{2v} symmetry. R is the distance between the centers-of-mass of the two monomer subunits. (e) Pictorial representation of the unit cell of crystalline CO_2 (Ref. 52). The unit cell of crystalline N_2O is analogous (Ref. 52).

In a first step, the optimized geometry and the harmonic fundamental wave numbers and intensities of the isolated molecule have been determined for all methods and basis sets. The different aggregates discussed in Sec. III were then built up by putting together the optimized monomers. For the aggregates again, harmonic fundamentals and intensities have been calculated at the same level of theory as for the monomer. These aggregates do not correspond for all cases to minimum structures, which could in principle lead to problems with the harmonic approximation assumed in the quantum chemical calculations. The intermolecular frequencies of the aggregates, however, are up to two orders of magnitude lower than the intramolecular stretching frequencies considered here. Thus, these two types of modes do not mix. With respect to the intramolecular stretching vibrations, the aggregates are near their minimum because the change in geometry of the individual molecules upon aggregation is only minor. It certainly lies within the range of validity of the harmonic expansion of the potential. Therefore, the small

TABLE I. Structural parameters (R, θ) for the experimental slipped-(anti)parallel dimers of CO_2 and N_2O depicted in Figs. 1(a) and 1(b), respectively. $\tilde{\nu}_D - \tilde{\nu}_M$ is the shift of the transition wave number between dimer and monomer. Column five lists the experimental values and column six contains the values obtained from exciton calculations. The vibrational bands of the dimers are labeled analogous to the corresponding vibrational bands of the monomers (ν_3: antisymmetric stretching vibration of CO_2 and N–N-stretching vibration of N_2O, respectively; ν_1: N–O-stretching vibration of N_2O).

		Experiment			Exciton approach
	Band	R/Å	θ/°	$\tilde{\nu}_D - \tilde{\nu}_M$/cm^{-1}	$\tilde{\nu}_D - \tilde{\nu}_M$/cm^{-1}
$(CO_2)_2$:	ν_3	3.6023(2)[a]	57.96(2)[a]	1.63[d]	1.76[g]
$(N_2O)_2$:	ν_3	3.4225(5)[b]	61.00(2)[b]	5.7[e]	2.3[h]
	ν_1	3.419(2)[c]	61.2(3)[c]	−5.2[f]	0.6[i]

[a]Reference 4.
[b]Reference 9.
[c]Reference 10.
[d]References 4 and 43.
[e]References 9 and 44.
[f]References 10 and 45.
[g]Reference 43.
[h]References 44 and 46.
[i]References 45 and 46.

deviations from the true equilibrium geometry do not affect the calculations of normal frequencies for the intramolecular vibrations.

The transition wave number $\tilde{\nu}_M$ and the transition dipole moment d_M of the isolated molecule calculated with the different quantum chemical methods are used as the input parameters for the corresponding exciton calculations [Eqs. (8) and (9)]. The comparison of the quantum chemical calculations with the exciton calculations then allows to decide to what extend the vibrational spectrum of the aggregates is determined by resonant dipole–dipole coupling.

III. COMPARISON WITH DIFFERENT CLUSTERS

A. Experimental dimers

The best way to test a model is to compare it with corresponding experimental data. For CO_2 and N_2O, however, complete experimental data for aggregates which are determined independently from the exciton model are only available for dimers.[4,9,10] The experimental minimum structures of $(CO_2)_2$ and $(N_2O)_2$ are shown in Figs. 1(a) and 1(b), respectively. The corresponding geometry parameters are listed in Table I. The shifts of the band centers between dimer[4,9,10] and monomer[43–45] $\tilde{\nu}_D - \tilde{\nu}_M$ are listed in the fifth column. From the experimental geometries of the dimers (R, θ), the experimental transition wave numbers of the monomers $\tilde{\nu}_M$, and the transition dipole moments of the monomers d_M,[43,46] we have calculated the transition wave numbers of the dimers within the exciton model as described in Sec. II A. The corresponding wave number shifts with respect to the monomer are listed in the last column of Table I. Note, that for the dimers only the transition to the vibrational state with u-symmetry is infrared active. The transition to the g-state is infrared inactive and thus is not considered here.

For the ν_3-band of $(CO_2)_2$, the experimental wave number shift between the dimer and the monomer is almost perfectly reproduced by the exciton model (Table I). This good agreement found for the dimer was the justification to use the exciton model to extract structural parameters for the trimer from its infrared spectrum as reported in a previous study by Nesbitt and co-workers.[47]

In the case of the ν_3-band of $(N_2O)_2$, the shift arising from the dipole–dipole coupling explains at least part of the experimentally observed shift. The negative shift of the ν_1-band, however, cannot be understood in the framework of the exciton model. For the experimental geometry of this dimer, the model always predicts a positive shift. The shift for the ν_1-band due to the dipole–dipole coupling is smaller than that for the ν_3-band by a factor of 3.7. This is due to the smaller transition dipole moment of the ν_1-band ($d_M = 0.130$ D) compared with the ν_3-band ($d_M = 0.249$ D).[46] The data in Table I clearly show that for the N_2O dimer further interactions other than simple dipole–dipole coupling have to be considered to explain the experimental shifts satisfactorily.

B. Dimers from quantum chemical calculations

There exist several theoretical studies for N_2O and CO_2 dimers in the literature (Refs. 15, 48–51, and references therein). To be able to relate quantum chemical calculations to the exciton model, we have determined optimized geometries, harmonic transition wave numbers, and intensities for the monomers and the slipped-(anti)parallel dimers shown in Figs. 1(a) and 1(b). The optimized geometry parameters and the wave number shifts between monomer and dimer $\tilde{\nu}_D - \tilde{\nu}_M$ for the fundamental stretching-modes are listed in Table II for various methods and basis sets. The corresponding shifts obtained with the exciton model are summarized in the last column of Table II. For these exciton calculations, the optimized geometries of the dimers (R and θ) and the transition wave number $\tilde{\nu}_M$ of the monomer and the transition dipole moment d_M of the monomer have been taken from the corresponding quantum chemical calculations.

For the CO_2 dimer, the experimental geometry in Table I is best reproduced by the MP2/6–31+G* level of theory. The wave number shifts, both calculated *ab initio* and with the exciton model, agree quite well with the experimental shift in Table I. In contrast, the optimized geometries calculated with AM1 and B3LYP differ clearly from the experimental geometry but, for the purposes considered in this study, this is not of further importance. Here, we are mainly interested in the comparison between wave number shifts on

TABLE II. The same as in Table I but for the slipped-(anti)parallel dimers [Figs. 1(a) and 1(b)] which correspond to the minimum structures of the different quantum chemical calculations.

			Quantum chemistry			Exciton approach
			Geometry		Shift	Shift
		Band	R/Å	θ/°	$\tilde{\nu}_D-\tilde{\nu}_M$ /cm^{-1}	$\tilde{\nu}_D-\tilde{\nu}_M$ /cm^{-1}
$(CO_2)_2$:	AM1	ν_3	4.3089	46.63	−3.05	−3.86
	B3LYP/6-31+G*	ν_3	3.9462	54.98	0.55	0.11
	B3LYP/aug-cc-pvtz	ν_3	3.9804	54.85	0.23	0.05
	MP2/6-31+G*	ν_3	3.6067	58.12	2.05	1.64
	MP2/aug-cc-pvtz	ν_3	3.4888	59.44	2.57	2.55
$(N_2O)_2$:	AM1	ν_3	3.3706	56.24	6.09	0.82
		ν_1			−5.48	0.31
	B3LYP/6-31+G*	ν_3	3.6874	58.37	4.87	1.13
		ν_1			−3.83	0.35
	B3LYP/aug-cc-pvtz	ν_3	3.7174	58.65	5.49	1.24
		ν_1			−4.07	0.39
	MP2/6-31+G*	ν_3	3.4060	60.32	−3.87	2.08
		ν_1			−0.39	0.12
	MP2/aug-cc-pvtz	ν_3	3.3279	61.31	−3.17	2.75
		ν_1			−1.09	0.18

the one hand calculated *ab initio* and on the other hand calculated with the exciton model. And as can be seen from Table II for $(CO_2)_2$, the order of magnitude of these shifts is indeed nicely reproduced by the exciton approach for all quantum chemical methods considered there. The negative shift obtained in the AM1 calculation is also reproduced, as is the only small shift calculated with the B3LYP functional. The latter is so small because the B3LYP equilibrium structures feature an angle θ very close to the magic angle $\theta_m \approx 54.7°$, for which the dipole–dipole coupling vanishes. The wave number shifts are negative for angles $\theta < \theta_m$ and positive for angles $\theta > \theta_m$. The last column in Table II clearly documents how sensitively the dipole–dipole coupling depends on the intermolecular geometry. At this point, we conclude that for the slipped-parallel dimer of CO_2, the agreement for the wave number shifts between quantum chemistry and exciton model is better than 1 cm^{-1}.

The situation for the N_2O-dimer is quite different. Again the experimental geometry of this dimer is best reproduced by the MP2/6–31+G* calculation. The corresponding *ab initio* value for the wave number shift $\tilde{\nu}_D-\tilde{\nu}_M$, however, does not agree well with the experimental value. For the AM1 and the B3LYP method the shifts are in better agreement with the experiment but only at the cost of a larger deviation for the geometry. The typical deviations for the transition wave numbers for the slipped-antiparallel dimer lie around 5 cm^{-1}—comparable to the shift itself. The comparison between quantum chemistry and exciton model seems at first sight rather discouraging.

The slipped-(anti)parallel dimer, however, is only one of the many possible spatial arrangements of two individual molecules in the huge aggregates considered in this study. For this specific dimer geometry the splitting caused by the exciton coupling is rather small (see Tables I and II) because the equilibrium angle θ lies near the magic angle for which the dipole–dipole coupling vanishes. By contrast, typical wave number shifts observed in the experimental spectra of nanoparticles are by more than a factor of ten larger (see, for instance, Refs. 24 and 25, and Sec. IV). Thus, the exciton model's suitability to describe band shapes in the infrared spectra of CO_2 and N_2O nanoparticles cannot be judged on the performance for the slipped-(anti)parallel dimer alone. Therefore, we have also tested other geometries. Table III summarizes the results for a parallel arrangement of the molecules. The corresponding geometries are depicted in Figs. 1(c) and 1(d). For these arrangements, the wave number shifts amount to about half the experimental shifts typically observed in the spectra of CO_2 and N_2O nanoparticles.

For $(CO_2)_2$, the agreement between the exciton model and the different quantum chemical methods is very good. As for the slipped-parallel dimer, the deviation of the exciton calculations decreases with increasing level of theory of the quantum chemical calculation. The results summarized in Tables I–III show that for this dimers the contributions arising from interactions other than the dipole–dipole coupling typically lie below 2 cm^{-1}. This result is also confirmed by similar calculations for the T-shaped dimer and by calculations for the symmetric stretching vibration of CO_2. The shifts calculated for these cases can only arise from such contribution because the dipole–dipole coupling vanishes here. Columns five and six in Table III contain the ratios of the integrated line strengths of dimer and monomer [see Eq. (7)]. The agreement between quantum chemical methods and exciton calculations is quite good. In summary, the results presented for the different CO_2 dimers reveal the dipole–dipole coupling as the dominant contribution to the infrared spectra.

The results for the N_2O-dimers are not so clear-cut. Apparently, the contributions of terms other than dipole–dipole interaction depend more sensitively on the intermolecular arrangement (see Tables I–III). From the data for $(N_2O)_2$, we conclude that the dipole–dipole coupling is the dominant contribution to the infrared spectra when the corresponding splitting exceeds about 5 cm^{-1}. This value corresponds to the

TABLE III. Shifts of the transition wave numbers between dimers and monomers, $\tilde{\nu}_D - \tilde{\nu}_M$, for the parallel dimers of CO_2 and N_2O shown in Figs. 1(c) and 1(d), respectively. Quantum chemical calculations on different levels of theory are compared with the corresponding exciton calculations. S_D/S_M is the ratio of the integrated line strengths of dimer and monomer [see Eq. (7)].

		Band	Quantum chemistry $\tilde{\nu}_D - \tilde{\nu}_M$ /cm^{-1}	Exciton approach $\tilde{\nu}_D - \tilde{\nu}_M$ /cm^{-1}	Quantum chemistry S_D/S_M	Exciton approach S_D/S_M
$(CO_2)_2$:	AM1	ν_3	13.03	17.35	1.7	2.0
	B3LYP/6-31+G*	ν_3	11.55	12.83	1.7	2.0
	B3LYP/aug-cc-pvdz	ν_3	11.98	12.87	1.7	2.0
	B3LYP/aug-cc-pvtz	ν_3	12.06	13.19	1.7	2.0
	B3LYP/aug-cc-pvqz	ν_3	12.07	13.19	1.7	2.0
	MP2/6-31+G*	ν_3	11.00	10.99	1.7	2.0
	MP2/aug-cc-pvdz	ν_3	11.46	11.18	1.7	2.0
	MP2/aug-cc-pvtz	ν_3	11.26	11.26	1.7	2.0
	MP2/aug-cc-pvqz	ν_3	11.32	11.31	1.7	2.0
$(N_2O)_2$:	AM1	ν_3	7.83	9.93	1.7	2.0
		ν_1	2.33	3.78	1.6	2.0
	B3LYP/6-31+G*	ν_3	7.95	7.53	1.6	2.0
		ν_1	2.32	2.31	1.6	2.0
	B3LYP/aug-cc-pvtz	ν_3	9.35	7.92	1.7	2.0
		ν_1	2.39	2.49	1.6	2.0
	MP2/6-31+G*	ν_3	10.91	7.25	1.6	2.0
		ν_1	0.75	0.42	1.5	2.0
	MP2/aug-cc-pvtz	ν_3	10.25	7.66	1.6	2.0
		ν_1	0.69	0.51	1.6	2.0

typical error to be expected for the exciton model for these aggregates.

C. Chains and small crystalline aggregates

Although the exciton model used here is essentially based on two-body interactions, the comparison only with dimers is not sufficient to verify the exciton approach for larger aggregates. In larger systems, the two-level resonance of the dimers is replaced by a cascade of many resonant levels. This is illustrated for different chains which consists of up to $N=10$ parallel CO_2 molecules. The arrangement of the individual molecules is analogous to that in the dimer depicted in Fig. 1(c). The calculated infrared spectra for these chains in the region of the antisymmetric stretching band are shown in the form of stick spectra in Fig. 2. Fat sticks represent the spectra calculated within the exciton approximation and thin sticks correspond to quantum chemical calculations. Note that the intensities of the weak transitions are scaled by a factor of 10 or 100 as indicated.

Figure 2 nicely shows that the absolute values of the mean wave number shifts relative to the monomer increases with the size of the aggregates. This is caused by a cascade of several resonant levels—a phenomenon which can obviously arise only in larger aggregates. This, however, does not lead to additional errors. The agreement between the exciton calculations and the quantum chemical calculations is of similar quality as found for the different dimers. Again, it improves with increasing level of theory. The accuracy for individual transition wave numbers for the different methods lies here around 5 cm^{-1}. Relative intensities of different transitions are reproduced clearly better than to within a factor of 2. From these results, we conclude that the exciton approach is able to reproduce the overall bandwidth as well as the coarse band structure in the infrared spectra of these larger aggregates.

These conclusions are also confirmed by calculations for small crystalline aggregates. These structures are built up from crystalline unit cells.[52] A scheme of the unit cell is shown in Fig. 1(e). The infrared spectra of two specific aggregates, one consisting of $2\times1\times1$ unit cells (8 molecules) and the other consisting of $3\times2\times2$ unit cells (48 molecules), are shown in Fig. 3. The exciton calculations are depicted in the lower traces and the semiempirical AM1 calculations are shown in the upper traces. All spectra are convoluted with a Gaussian of 2 cm^{-1}. For the aggregate consisting of $2\times1\times1$ unit cells, we have also performed B3LYP/6–31+G* calculations with results similar to those shown in Fig. 3 for AM1. The agreement between the exciton calculations and the AM1 calculations in Fig. 3 is consistent with the corresponding results obtained above for the other aggregates. It is clear that the deviations expected for the exciton model have the most pronounced effect for the ν_1-band of N_2O (traces c and f in Fig. 3). This band is comparatively narrow with an overall band width around 15 cm^{-1}. Therefore, deviations on the order of 5 cm^{-1} can have an appreciable influence on the overall width as well as on the band structure.

From the results obtained in this section, we finally conclude that the exciton approximation is indeed good enough to describe the main features in the infrared spectra of large aggregates of CO_2 and N_2O. Variations in the band structure which are smaller than 5 cm^{-1}, however, have to be interpreted with care. This is particularly important for the analysis of the ν_1-band of N_2O particles.

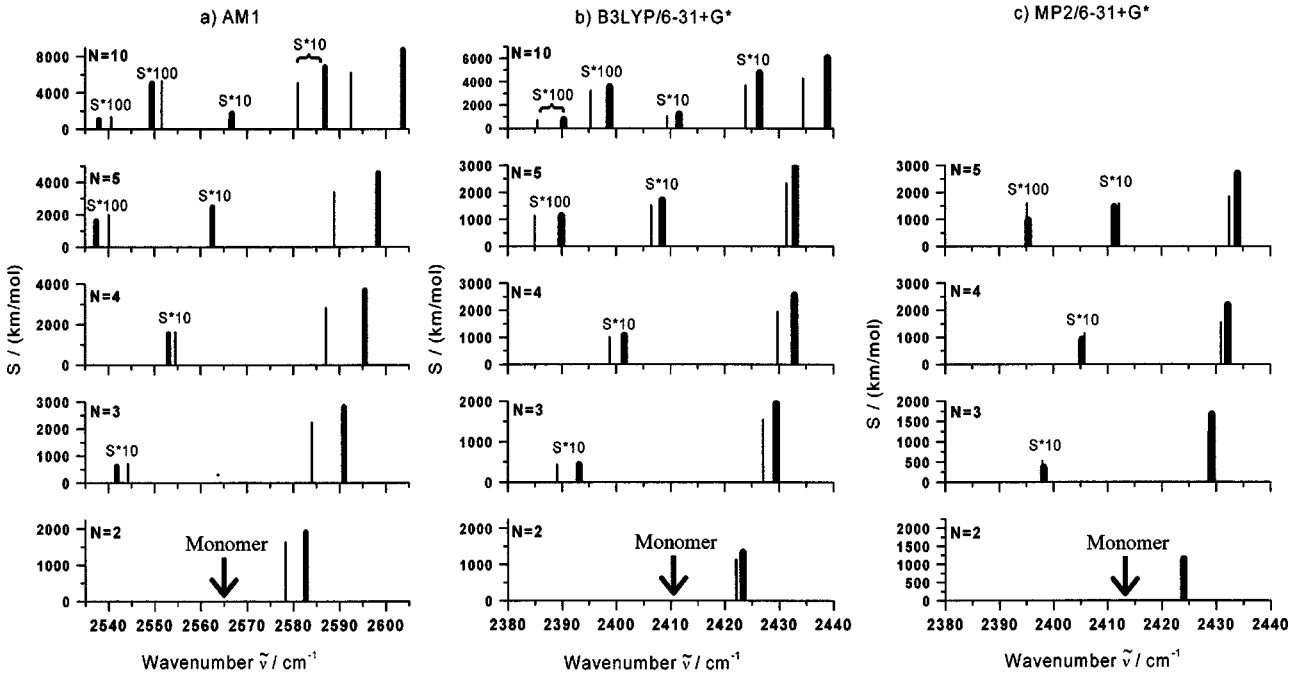

FIG. 2. Infrared spectra of parallel CO_2 molecules arranged in a chain with a total of $N=2$, 3, 4, 5, and 10 molecules (from bottom to top). The spectra are displayed in form of stick spectra. Fat lines: Exciton calculations. Thin lines: Quantum chemical calculations [(a) AM1; (b) B3LYP/6–31+G*; (c) MP2/6–31+G*]. The transition wave numbers of the isolated molecules $\tilde{\nu}_M$ are indicated by arrows (AM1: $\tilde{\nu}_M=2565.3$ cm^{-1}; B3LYP: $\tilde{\nu}_M=2410.5$ cm^{-1}; MP2: $\tilde{\nu}_M=2413.0$ cm^{-1}). Note that the intensities of the weak transitions are scaled by a factor of 10 or 100.

IV. EXCITON CALCULATIONS FOR NANOPARTICLES

A. Dependence on particle shape and size

The aggregates which have been discussed until now have spatial dimensions of up to 1 nm. Concerning the accuracy of the exciton approximation, the results obtained for these aggregates can also be transferred to larger particles since there are no fundamental changes. However, other questions remain to be answered when the exciton approach is used for particles with typical dimensions between 1 and 10 nm. One concerns the relation of the accuracy of the exciton approximation to the typical spectral changes arising from different particle shapes or different particle sizes. It is obviously essential to clarify this point if such particle properties are to be determined from the comparison of the simulated and the experimental spectrum.

We have found very pronounced spectral changes for different particle shapes. This is illustrated in Fig. 4 for three aggregates with different shapes but with the same number of CO_2 molecules (see figure caption). As input parameters for the exciton calculations [see Eqs. (8) and (9)], we have used here the corresponding experimental values of the free CO_2 monomer.[43] The spectral changes arising from different

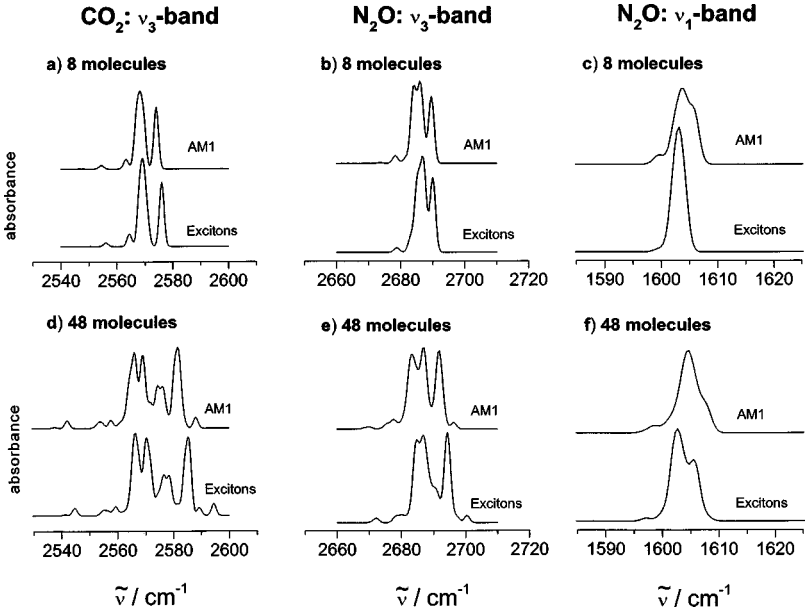

FIG. 3. Infrared spectra of crystalline CO_2 and N_2O clusters. Panels (a), (b), and (c): Arrangement of $2\times1\times1$ unit cells containing 8 molecules. Panels (d), (e), and (f): Arrangement of $3\times2\times2$ unit cells containing 48 molecules. Upper traces: AM1 calculations. Lower traces: Exciton calculations. Panels (a) and (d): Antisymmetric stretching vibration of CO_2. Panels (b) and (e): N–N-stretching vibration of N_2O. Panels (c) and (f): N–O-stretching vibration of N_2O. The spectra are convoluted with a Gaussian band shape of 2 cm^{-1}.

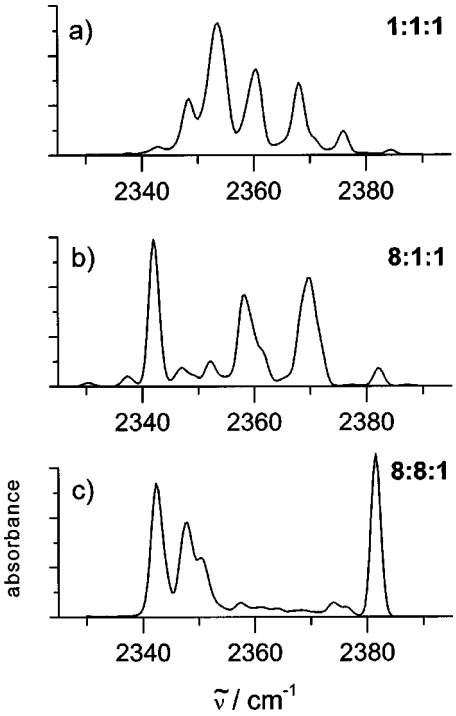

FIG. 4. Infrared spectra of crystalline CO_2 particles with different shape but the same number number of molecules $N=2048$. The spectra were calculated within the exciton approximation. (a) Arrangement of $8\times8\times8$ unit cells. (b) Arrangement of $32\times4\times4$ unit cells. (c) Arrangement of $16\times16\times2$ unit cells. The corresponding axis rations are indicated in the figure. The spectra are convoluted with a Gaussian band shape of 2 cm^{-1}. As input parameters for the exciton calculations [see Eqs. (8) and (9)], the experimental values of the gas phase molecules were used (Ref. 43).

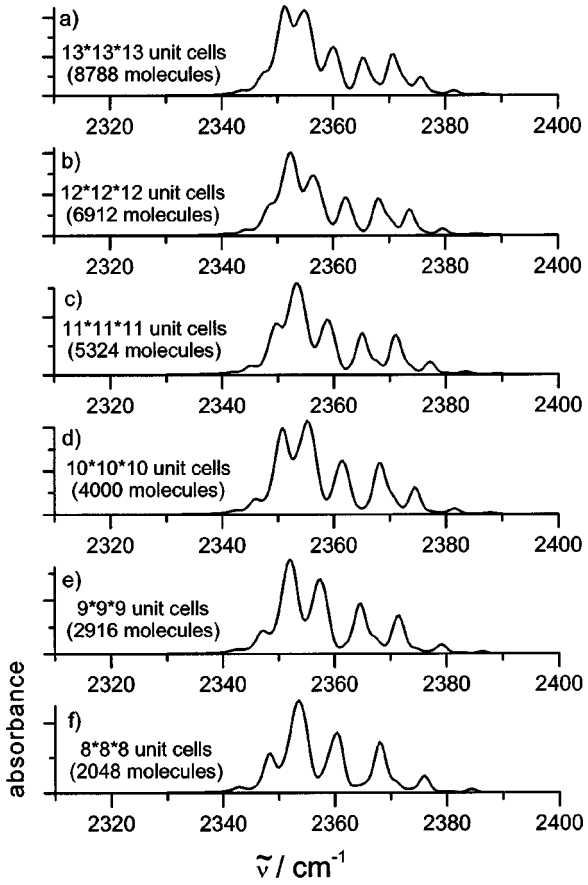

FIG. 5. Infrared spectra of crystalline CO_2 particles with different size but the same shape (arrangements of $x\times x\times x$ unit cells). The spectra were calculated within the exciton approximation. The particle size decreases from panel (a) to panel (f) as indicated. For these calculations, the same parameters as in Fig. 4 were used.

particle shapes far exceed the uncertainties expected for the exciton approximation. Thus, with the help of simulated spectra it should be possible to distinguish between different particle shapes directly from experimental infrared spectra. There are two effects which contribute to the distinct shape-dependence. One is the huge surface to volume ratio of nanoparticles. Consequently, the spectra of these particles are strongly influenced by the characteristic absorptions of the molecules in the surface layer. The other effect is caused by the long-range influence of the dipole–dipole coupling which is discussed in the next subsection. For particles below 10 nm, the effective range of the coupling is comparable to the particle's dimension.

The size-dependence of the spectra of particles in the range of 1–10 nm is less pronounced than the shape-dependence. For particles containing less than about 2000 molecules, the spectral changes are sufficiently pronounced to distinguish between different particle sizes from the band shapes in the infrared spectra. With increasing particle size, however, the size-dependence of the spectra decreases. For particles with more than 2000 molecules, one observes spectral changes on the same order of magnitude as the accuracy estimated above for the exciton approach. Here, the particle size can no longer be determined solely from the band shapes in the infrared spectra. This is illustrated in Fig. 5 for a series of spectra of crystalline CO_2 particles with different sizes (see figure caption). The results obtained in this subsection for CO_2 particles are also valid for N_2O particles. For the reasons discussed above, the band shape of the ν_1-band has to be interpreted with care.

B. Long-range influence of the dipole–dipole coupling

The Hamiltonian in Eq. (3) includes the dipole–dipole interaction between all $N(N-1)/2$ pairs of molecules in the particle. The interaction between two specific molecules changes as $1/r_{ij}^3$ with their distance r_{ij}. This decrease of the coupling matrix element with increasing distance is partially balanced by an increase in the radial density of coupling partners with increasing distance. In a particle of finite size, however, the number of coupling partners for each specific molecule depends on its spatial position in the particle. Or in other words, it depends on the particle's size and shape.

To find out how large the effective range of the dipole–dipole coupling is compared with the particle dimension, we have successively decreased the number of coupling partners considered for each molecule. For each molecule only the couplings to other molecules which lie within a sphere of a given radius r are considered. The infrared spectrum $f(\tilde{\nu})$ calculated in this way (reduced calculation) is then compared with the corresponding infrared spectrum $g(\tilde{\nu})$ for a full cal-

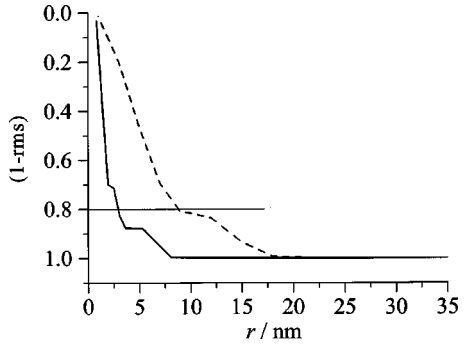

FIG. 6. Overlap (1-rms) between full and reduced exciton calculations as a function of the radius r [see Eq. (10)]. r corresponds to the maximum distance within which couplings are considered for the reduced calculations. Full Line: one-dimensional particle ($50\times1\times1$ unit cells). Dashed line: two-dimensional particle ($47\times47\times1$ unit cells). An overlap of 0.8 corresponds to a deviation of the spectra on the order of the estimated accuracy of the exciton approach.

culation, i.e., one which includes all pair interactions. As a measure for the deviation between the two spectra, we define an overlap (1-rms) as follows:

$$(1-\mathrm{rms})=1-\frac{\sqrt{\int(f(\tilde{\nu})-g(\tilde{\nu}))^2d\tilde{\nu}}}{\sqrt{\int f(\tilde{\nu})^2d\tilde{\nu}+\int g(\tilde{\nu})^2d\tilde{\nu}}}. \tag{10}$$

For identical spectra $f(\tilde{\nu})$ and $g(\tilde{\nu})$ the overlap equals 1.

To determine the radius of influence of the dipole–dipole coupling itself, a one-dimensional particle is best suited. Here, the radial density of coupling partners has a constant value for all distances. As an example, we use a needlelike arrangement of $50\times1\times1$ unit cells. This particle has a long axis of about 30 nm and two short axes of less than one nanometer. The overlap with the full calculation as a function of the radius r is shown in Fig. 6 (full line). Above a radius of about 8 nm the overlap nearly reaches its maximum. For the present study, a deviation from the spectra of the reduced and the full calculation becomes relevant if it is on the same order as the accuracy estimated for the exciton approach in Sec. III. This typically corresponds to a value of about 0.8 for the overlap. As indicated by the thin horizontal line in Fig. 6, this limit is reached for a radius $r\approx3$ nm. Therefore, the effective range of the dipole–dipole coupling itself extends over about 6 unit cells. For the corresponding reduced calculation only a fifth of all possible pair interactions had to been included.

The influence of the increase in the density of coupling partners with increasing distance becomes evident only for two and three-dimensional particles. The results for a two-dimensional particle consisting of $47\times47\times1$ unit cells (long axes ≈35 nm) are represented by the dashed line in Fig. 6. In this case, the typical effective range of the dipole–dipole coupling amounts to about 9 nm. In a three-dimensional particles it lies even above 10 nm. This value corresponds to the maximum particle dimension considered in this study. This means that for particles below 10 nm all pair interactions through the whole particle have to be included in the exciton calculations for reliable result.

V. SUMMARY

In the present study, we have investigated the suitability of the vibrational exciton approach to describe the characteristic band shapes in the infrared spectra of CO_2 and N_2O nanoparticles. The spatial dimensions of the particles investigated typically lie between 1 and 10 nm. The study focuses on the region of the intramolecular stretching vibrations. For the isolated molecules, the corresponding fundamental transitions have quite large transition dipoles. Thus, the resonant dipole–dipole coupling between the individual molecules is expected to be one of the dominant contributions to the vibrational spectra of CO_2 and N_2O nanoparticles.

From the comparison with experimental data and quantum chemical calculations for various small clusters, we estimate that the transition wave numbers of individual vibrational transitions in the particle spectra are described by the exciton approximation with an accuracy of better than 5 cm^{-1}. The relative transition intensities of different transitions are reproduced better than to within a factor of 2. The estimated accuracy has to be related to the typical splittings expected for the stretching bands of the particles. For the strong ν_3-bands, i.e., the antisymmetric stretching vibration of CO_2 and the N–N stretching vibration of N_2O, this leads to the conclusion that the characteristic band structures in the particle spectra are mainly determined by the resonant dipole–dipole coupling. For these bands, the exciton approach is suitable to analyze the band structures and the overall band widths in the particle spectra. For the band shape of the weaker ν_1-band of N_2O (N–O stretching vibration), however, the influence of the dipole–dipole coupling is not always dominant. An interpretation of this band within the exciton approach is only possible in conjunction with the stronger ν_3-band always paying attention to the consistency of the conclusions.

The exciton calculations for CO_2 and N_2O nanoparticles show that in the region below 10 nm the spectral changes due to different particle shapes are very pronounced—at least for the crystalline systems studied here. In contrast, the spectral changes due to different particle sizes are distinct only for particles containing less than about 2000 molecules ($\sim$5 nm). These effects are closely related to the effective range of the dipole–dipole coupling. For the nanoparticles considered in this study, it is comparable to the particles' dimension.

In conclusion we find the exciton approach suitable to analyze the infrared spectra of particles for sufficiently strong transitions ($\mu>0.2$ D). The interpretation of the structure of weaker bands may still be possible through comparison with the simultaneous analysis of the stronger bands. Encouraged by these results, we will use the exciton model to analyze the infrared spectra of nanoparticles measured earlier in our group.[24,31,53] The sizes of these particles lie between 1 and 10 nm, where infrared spectra can be modeled neither by quantum chemical methods nor by continuum models. This size range becomes accessible through the exciton approach. Extensions of the approach will include further interactions, e.g., dipole-induced dipole interactions,[41] as well as methods to treat even larger systems ($>10^4$ molecules). This will allow us to bridge the gap between quan-

tum chemical calculations and continuum models for particulate systems. For the latter, this eventually provides a check of the consistency with microscopic descriptions.

ACKNOWLEDGMENTS

This work was supported by the Deutschen Forschungsgemeinschaft (Grant No. SI 833/1–1) and the Fonds der Chemischen Industrie.

[1] A. A. Vigasin, F. Huisken, A. I. Pavlyuchko, L. Ramonat, and E. G. Tarakanova, J. Mol. Spectrosc. **209**, 81 (2001).
[2] E. Knözinger and P. Beichert, J. Phys. Chem. **99**, 4906 (1995).
[3] K. W. Jucks, Z. S. Huang, R. E. Miller, G. T. Fraser, A. S. Pine, and W. J. Lafferty, J. Chem. Phys. **88**, 2185 (1988).
[4] M. A. Walsh, T. H. England, T. R. Dyke, and B. J. Howard, Chem. Phys. Lett. **142**, 265 (1987).
[5] G. A. Pubanz, M. Maroncelli, and J. W. Nibler, Chem. Phys. Lett. **120**, 313 (1985).
[6] T. E. Gough, R. E. Miller, and G. Scoles, J. Phys. Chem. **85**, 4041 (1981).
[7] M. J. Weida and D. J. Nesbitt, J. Chem. Phys. **105**, 10210 (1996).
[8] G. T. Fraser, A. S. Pine, W. J. Lafferty, and R. E. Miller, J. Chem. Phys. **87**, 1502 (1987).
[9] H.-B. Qian, W. A. Herrebout, and B. J. Howard, Mol. Phys. **91**, 689 (1997).
[10] Y. Ohshima, Y. Matsumoto, and M. Takami, Chem. Phys. Lett. **152**, 294 (1988).
[11] Z. S. Huang and R. E. Miller, J. Chem. Phys. **89**, 5408 (1988).
[12] M. Gauthier, J. Chem. Phys. **88**, 5439 (1988).
[13] R. E. Miller, R. O. Watts, and A. Ding, Chem. Phys. **83**, 155 (1984).
[14] T. E. Gough, R. E. Miller, and G. Scoles, J. Chem. Phys. **69**, 1588 (1978).
[15] S. Kudoh, K. Onoda, M. Takayanagi, and M. Nakata, J. Mol. Struct. **524**, 61 (2000).
[16] R. E. Miller and L. Pedersen, J. Chem. Phys. **108**, 436 (1998).
[17] R. E. Miller and L. Pedersen, Chem. Phys. Lett. **275**, 307 (1997).
[18] S. I. Kovalenko, D. D. Solnyshkin, E. T. Verkhovtseva, and V. V. Eremenko, Low Temp. Phys. **27**, 681 (2001).
[19] G. Torchet, M.-F. Feraudy, A. Boutin, and A. H. Fuchs, J. Chem. Phys. **105**, 3671 (1996).
[20] H.-D. Barth and F. Huisken, Chem. Phys. Lett. **169**, 198 (1990).
[21] G. E. Ewing and D. T. Sheng, J. Phys. Chem. **92**, 4063 (1988).
[22] J. A. Barnes and T. E. Gough, J. Chem. Phys. **86**, 6012 (1987).
[23] G. D. Stein and J. A. Armstrong, J. Chem. Phys. **58**, 1999 (1973).
[24] M. K. Kunzmann, R. Signorell, M. Taraschewski, and S. Bauerecker, Phys. Chem. Chem. Phys. **3**, 3742 (2001).
[25] Th. Häber, U. Schmitt, C. Emmeluth, and M. A. Suhm, Faraday Discuss. **118**, 331 (2001).
[26] S. Bauerecker, M. Taraschewski, C. Weitkamp, and H. K. Cammenga, Rev. Sci. Instrum. **72**, 3946 (2001).
[27] T. E. Gough and T. Wang, J. Chem. Phys. **105**, 4899 (1996).
[28] J. A. Barnes, T. E. Gough, and M. Stoer, J. Phys. Chem. **97**, 5495 (1993).
[29] R. Disselkamp and G. E. Ewing, J. Chem. Phys. **99**, 2439 (1993).
[30] F. Fleyfel and J. P. Devlin, J. Phys. Chem. **93**, 7292 (1989).
[31] M. K. Kunzmann, S. Bauerecker, M. A. Suhm, and R. Signorell (unpublished).
[32] M. A. Ovchinnikov and C. A. Wight, J. Chem. Phys. **99**, 3374 (1993).
[33] G. Cardini and V. Schettino, J. Chem. Phys. **94**, 2502 (1991).
[34] J. E. Cahill, J. Chem. Phys. **66**, 4847 (1977).
[35] V. Schettino and P. R. Salvi, Spectrochim. Acta, Part A **31**, 399 (1975).
[36] D. A. Dows and V. Schettino, J. Chem. Phys. **58**, 5009 (1973).
[37] D. Fox and R. M. Hexter, J. Chem. Phys. **41**, 1125 (1964).
[38] R. M. Hexter, J. Chem. Phys. **33**, 1833 (1960).
[39] M. A. Ovchinnikov and C. A. Wight, J. Chem. Phys. **100**, 972 (1994).
[40] R. Disselkamp and G. E. Ewing, J. Chem. Soc., Faraday Trans. **86**, 2369 (1990).
[41] G. Cardini, V. Schettino, and M. L. Klein, J. Chem. Phys. **90**, 4441 (1989).
[42] M. J. Frisch, G. W. Trucks, H. B. Schlegel *et al.*, GAUSSIAN 98, Revision A.7, Gaussian, Inc., Pittsburgh, PA, 1998.
[43] V. Malathy Devi, B. Fridovich, G. D. Jones, and D. G. S. Snyder, J. Mol. Spectrosc. **105**, 61 (1984).
[44] J. Plíva, J. Mol. Spectrosc. **12**, 360 (1961).
[45] R. P. Grosso and T. K. McCubbin, J. Mol. Spectrosc. **13**, 240 (1964).
[46] R. H. Kagann, J. Mol. Spectrosc. **95**, 297 (1982).
[47] M. J. Weida, J. M. Sperhac, and D. J. Nesbitt, J. Chem. Phys. **103**, 7685 (1995).
[48] R. Bukowski, J. Sadlej, B. Jeziorski, P. Jankowski, K. Szalewicz, S. A. Kucharski, H. L. Williams, and B. M. Rice, J. Chem. Phys. **110**, 3785 (1999).
[49] S. Tsuzuki, T. Uchimaru, M. Mikami, and K. Tanabe, J. Chem. Phys. **109**, 2169 (1998).
[50] L. M. Nxumalo, T. A. Ford, and A. J. Cox, J. Mol. Struct. **307**, 153 (1994).
[51] A. J. Illies, M. L. McKee, and H. B. Schlegel, J. Phys. Chem. **91**, 3489 (1982).
[52] R. W. G. Wyckoff, *Crystal Structures* (Wiley, New York, 1963), Vol. 1.
[53] M. K. Kunzmann, doctoral thesis, Cuvillier Verlag, Göttingen, 2002.